Transition Metal Oxides for Supercapacitors

A thesis submitted towards partial fulfillment of
BS-MS Dual Degree Programme

By

NITHINRAJ P.D.
(BS-MS student, Registration No.: 20121017)

Under the guidance of

Dr. Seema Verma

Department of Chemistry
Indian Institute of Science Education and Research (IISER) Pune, India

Certificate

This is to certify that this dissertation entitled "**Transition Metal Oxides for Supercapacitors**" towards the partial fulfillment of the BS-MS dual degree programme at the Indian Institute of Science Education and Research Pune, represents original research carried out by **Nithinraj P.D.** at IISER Pune under the supervision of "**Dr. Seema Verma**, Faculty Fellow, Department of Chemistry, IISER Pune" during the academic year of 2016-2017.

Seema Verma

Date: 20/3/2017
Pune: Pune

Dr. Seema Verma
Faculty Fellow
Department of Chemistry
IISER Pune

Declaration by the candidate

I hereby declare that the matter embodied in the report entitled "**Transition Metal Oxides for Supercapacitors**" are the results of investigation carried out by me at the department of chemistry, IISER Pune, Under the supervision of Dr. Seema Verma and the same has not been submitted elsewhere for any other degree.

NithinRaj P.D.

Date: 20-03-2017

20121017

Place: Pune

Acknowledgements

I would like to express my profound gratitude and deep regards to **Dr. Seema Verma** for continuous support, care and guidance throughout this project. I would also like to express my sincere gratitude to **Dr. Muhammed Musthafa** for his support, motivation and valuable advice throughout this project.

I am extremely thankful to **Dr. Ravi Kumar and Alagar Raja** for their help and advice during the electrochemical measurements.

I would like to express my special thanks to Anagha, Surya, Thasneem, Navathej, Anjana Raj and all my friends for their help, care and support throughout this project.

I would like to thank all lab mates especially Fawaz, Zahid, Pramod, Manu Gautham, Mruthunjayachari, Neethu for their cooperation and help in completing my project.

I would like to thank Sujith K Gosh group for providing BET measurement facilities for completing my project.

I am grateful to **IISER Pune**, Department of Chemistry, for providing an excellent research platform and facilities.

I take this opportunity to thank my family and friends for continuous support and encouragement.

Last but not the least, I thank each and everybody who helped me in making this project successful.

Contents

List of Illustrations

List of Abbreviations

FESEM - Field Emission Scanning Electron Microscope

XRD - X-ray Diffraction

SC - Supercapacitor

EC - Electrochemical Capacitor

EDLC - Electrochemical double layer capacitor

FC - Faradic capacitors

MTMO - Mixed Transition Metal Oxides

CV - Cyclic Voltammetry

TGA - Thermo Gravimetric Analysis

BET - Brunauer-Emmett-Teller

EASA - Electrochemically Active Surface Area

OCV - Open Circuit Voltage

SD - Self Discharging

LC - Leakage Current

Abstract

Transition metal oxides have been extensively studied for last few years for its vast potentials in energy storage and conversion applications due to its remarkable electrochemical properties, low cost and environmental friendliness. In this direction, ternary nickel cobaltite ($NiCo_2O_4$) nanocrystals have become a promising energy storage materials for supercapacitor application due to its prolific electroactive sites and higher electrical conductivity compared to the corresponding binary metal oxides. In the present project work, a simple and generally applicable strategy was developed for the efficient synthesis of nanostructured nickel cobaltite of varying morphologies simply by changing metal to urea ratio. In this direction, sustained and dedicated research efforts were devoted with an aim to achieve binderless hierarchical nanostructures directly on the nickel foam substrate. Cyclic voltammetry and galvanostatic charge-discharge measurements indicated an extremely high areal capacitance of 4349 mF/cm^2 for nickel cobalt oxide nanowires compared to other morphologies such as nanoneedles (2100 mF/cm^2), nanosheets with wires (2445 mF/cm^2) and platelets (968 mF/cm^2). Nickel cobaltite nanowire electrode demonstrated extended cyclability at 4 mA/cm^2 current density with more than 90% capacity retention at the end of 13000 cycles. To understand the intrinsic charge injection capability of different morphologies, the capacitance values are normalized with respect to electrochemically accessible area. The resulting true area normalized charge injection capability is more than doubled in nickel cobalt oxide nanowires compared to other morphologies. This indicates the exposure of more electroactive cationic sites at nickel cobalt oxide nanowire electrode/electrolyte interface towards tuning the interfacial charge storage mechanism. Investigation of supercapacitive failure mechanism by leakage current and self-discharge rate suggest the most probable failure pathway in nanowire morphology could be a charge redistribution rather than a parasitic Faradic redox chemistry.

CHAPTER 1

This chapter starts with a brief introduction to the energy storage and gives a critical review of the literature on supercapacitors and other energy storing devices in recent years. A brief review of the literature on the motivation behind the work is presented here. The importance of mixed ternary metal oxide having spinel structure mainly nickel cobaltite and the relevance of electrochemical studies in this material is discussed in the chapter.

1.1. Introduction

Rapid depletion of fossil fuels and growing environmental pollution due to the greenhouse gas emission are pushing scientists to exploit highly efficient technologies.[1-6] In spite of having numerous electrochemical energy storage/conversion systems, the widespread commercialization of the technologies is still greatly hampered due to their high cost, efficiency, operational problems which are ultimately related to severe materials challenges. Therefore, efforts are needed to search for commercially viable new materials of rational design that can lower the cost, increase the efficiency and improve the cycling stability.[1,3,5]

Li-ion batteries, fuel cells, and supercapacitors are the most popular energy storing devices.[5] The need of an alternative energy storing device for powering electric cars and other heavy electronic device are very challenging. Lithium ion batteries have high energy density with poor power density and cycle life where as supercapacitors have high power density and cycle life but poor energy density.[5] Current potential energy storage devices like Li-ion batteries, fuel cells and supercapacitors have to be improved to get better energy density and power density with high cycling stability. Fabricating new kinds of electrodes by choosing better electrode material and modifying it in nanoregime can increase the power and energy density.[2,4,5] Higher electrical conductivity, superior ion transport, fast electrode kinetics, high structural stability, low self-discharging and high cycle life can be achieved by suitably selecting the electrode material with desired morphology and size. Ragone plot is widely used to analyze and understand different energy storage devices. X axis represents the specific energy and Y axis represents the specific power.

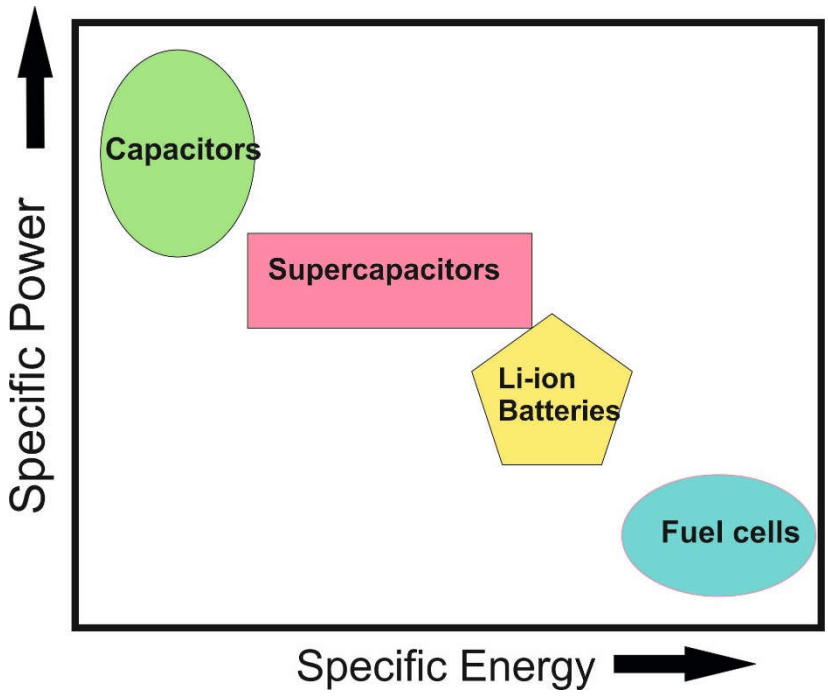

Figure 1.1: Ragone plot of fuel cells, lithium ion batteries, supercapacitors and capacitors

Figure 1.1 shows the Ragone plot of fuel cells, lithium ion batteries, supercapacitors and capacitors having specific energy on the X axis and specific power on the Y axis.

Supercapacitors (SC) having a high specific power and cycling life got more attraction in the recent years.[1-5,15] In this direction, transition metal oxides are extensively studied for last few years for its unlimited potentials in energy storage and conversion applications.[5] Although great progress has been made in recent years, they still suffer from deficiencies due to their lower capacitance, poor efficiency and limited cycling stability, which restrict their wide practical applications. Interestingly, the elegant mixing of transition metal oxide into unique spinel - like structures, leads to the formation of single phase mixed transition metal oxide ($A_xB_{3-x}O_4$) where A and B represents different transition metal cations.[5] Various cations with more than one oxidation states may be systematically distributed to the available octahedral and tetrahedral sites of fcc close-packed oxygen atoms. The presence of multiple valence metal cations decreases the

activation energy for charge transfer and thereby increases the electronic conductivity as twice as that of transition metal oxides. Moreover, buffering of volume due to the difference in expansion coefficient of metal cations, yield better cycling stability. The synergetic effect of the presence of two different metals in a single spinel-like phase (instead of having two different binary oxides) gives exceptionally high capacitance compared to that of other electrode materials.

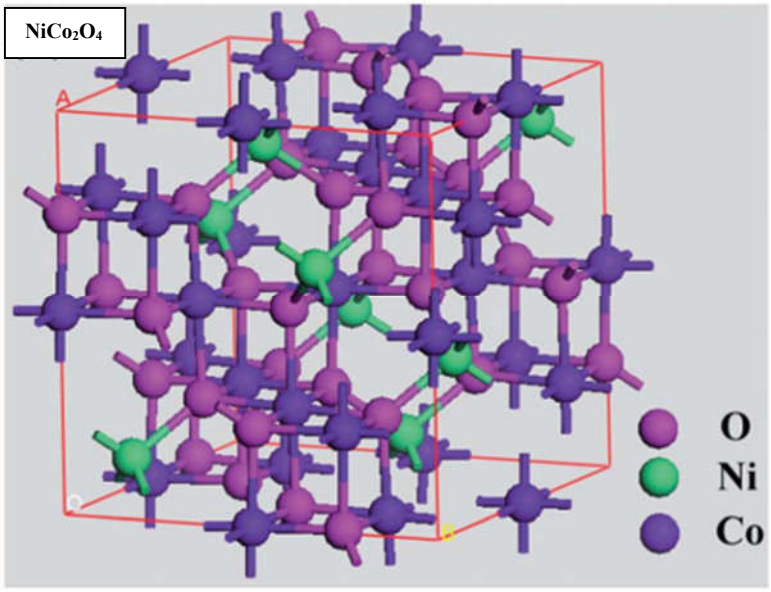

Figure 1.2: Crystal structure of nickel cobalt oxide.[17]

Among all mixed transition metal oxides nickel cobaltite ($NiCo_2O_4$) has been suggested as a promising cost-effective and scalable alternative candidate for SC because of its low cost, better electrical conductivity and higher electrochemical activity.[7,9,10] Nickel cobalt oxide can have variable oxidation states for nickel and cobalt metal ions and an uncertainty in the metal cation positions which enhances its pseudocapacitance properties compared to that of other mixed transition metal oxides. Nickel cobalt oxide is expected to offer richer redox reactions than those of the monometallic nickel oxides and cobalt oxide. In recent years many studies are reported to understand and improve the efficiency of this material for supercapacitor applications. Some papers talk about the supercapacitance in terms of increased surface area and optimum pore volume. Many studies show the direct relation of capacitance with superior morphologies and

hybrid materials. But basic electrochemical studies like electrochemically active surface area, leakage current, and self-discharging studies are rarely studied.

Nickel cobalt oxide can be synthesized by different methods like combustion reactions, hydrothermal reactions, microwave assisted synthesis and so on. We chose a simple hydrothermal method and subsequent thermal decomposition for synthesizing clean and monodispersed nanoparticles. We have successfully tuned different morphologies by just changing the metal to urea concentration. Electrochemical studies have been done by dropcasting slurry of the powdered sample along with a suitable binder and conducting material on top of glassy carbon. In order to avoid the effect of the binder, we have fabricated binder fee electrodes with better capacitance and cycling stability. Morphology of the materials has the crucial role in improving the electrochemical properties. In the present investigation, sustained and dedicated research efforts are devoted towards nanostructure designing which would help us in achieving increased active surface areas with short ion transport pathways, required for higher capacity/capacitance and understanding the effect of change in electrochemical properties in different morphologies.

1.2. Capacitors

A conventional capacitor consists of two parallel plates (electrodes) separated by an insulating dielectric material. When a potential difference is applied, the opposite charge gets accumulated on two electrode surfaces which polarize the dielectric material. The dielectric material separates this charge and an electric field is created which allows the capacitor to store energy.

Capacitance C is defined as the ratio of charge stored Q to the applied potential difference V.

$$\mathbf{C = Q / V}$$

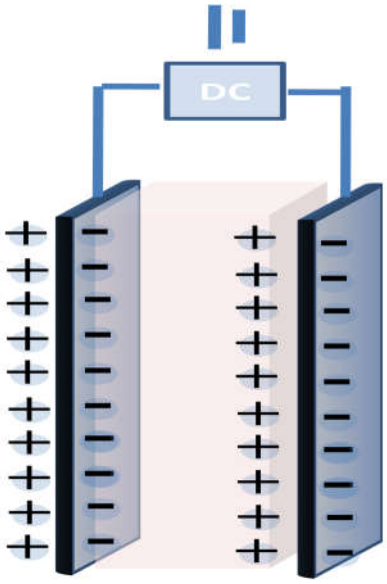

Figure 1.3: Schematic representation of parallel plate capacitor.

Capacitance is directly proportional to the area of electrode surface A, dielectric constant ε and inversely proportional to the distance between the electrodes d. Capacitance can be increased by increasing the electrode surface area or by decreasing the distance between the electrodes.

$$C = \varepsilon A / d$$

Energy stored in a capacitor is directly proportional to the capacitance of the capacitor.

$$E = CV^2/2$$

Conventional capacitors have very high power density but low energy density compared to batteries and fuel cells.

1.3. Supercapacitors (Electrochemical capacitors)

Supercapacitors are one of the most promising devices for storing electrical energy due to its high power density and cycling life.[15] Supercapacitors are mainly classified into two types (i) **Electrical double-layer capacitors (EDLC)** (Non-faradic capacitors), and (ii) **pseudocapacitors** (faradic capacitors).

1.4. Electrochemical double-layer capacitors (EDLC)

EDLC store charge on the surface of the electrode material in a non-faradaic way, i.e. there is no charge transfer through the electrode - electrolyte interface.[9] It consists of two high surface area carbon electrodes, an electrolyte and a separator. When a potential difference is applied, electrodes get oppositely charged and the ions in the electrolyte get attracted towards it. The ions get accumulated on the surface of the electrode with opposite charge. Figure 1.4 shows the working of EDLC.

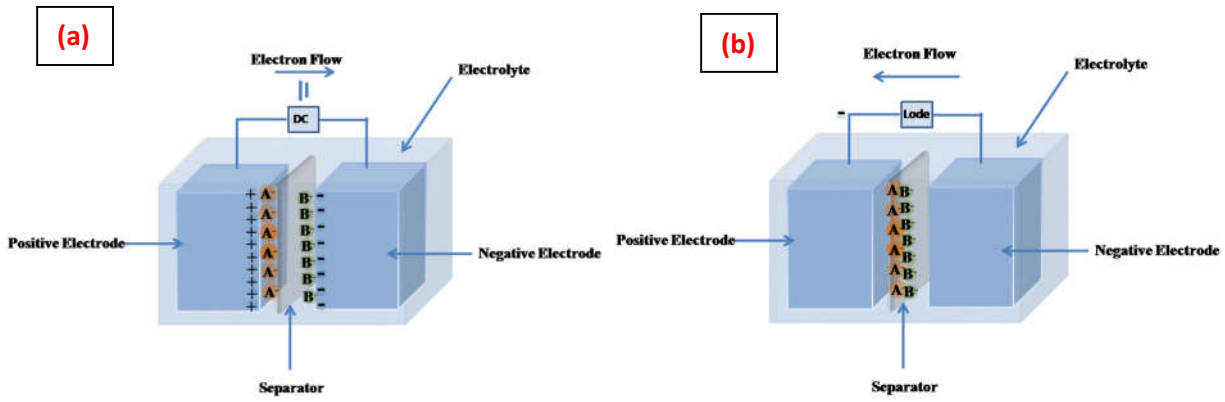

Figure 1.4: Schematic of electrical double layer capacitor (a) Charging (b) Discharging.

The capacitance of these supercapacitors increases with increase in surface area. Since this process does not create any chemical or compositional change to the electrode materials, these are highly reversible in nature and have high cycling stability. Porous carbon based materials are widely used as electrode material due to its high surface area with excellent chemical and mechanical stability.[16] They have high power density and cycling life. Activated carbon, carbon aerogels and carbon nanotubes are widely studied as promising EDLC material.

1.5. Pseudocapacitors (Faradic capacitors, FC)

Pseudocapacitors or faradic capacitors can store charge in a faradic manner. Charge transfer due to redox reaction will happen across the electrode-electrolyte interface.[1-3,5,15] They have high energy density compared to that of EDLC. Unlike batteries, the

redox reaction happens only on the surface of the electrode and not in the bulk which yields high power density.

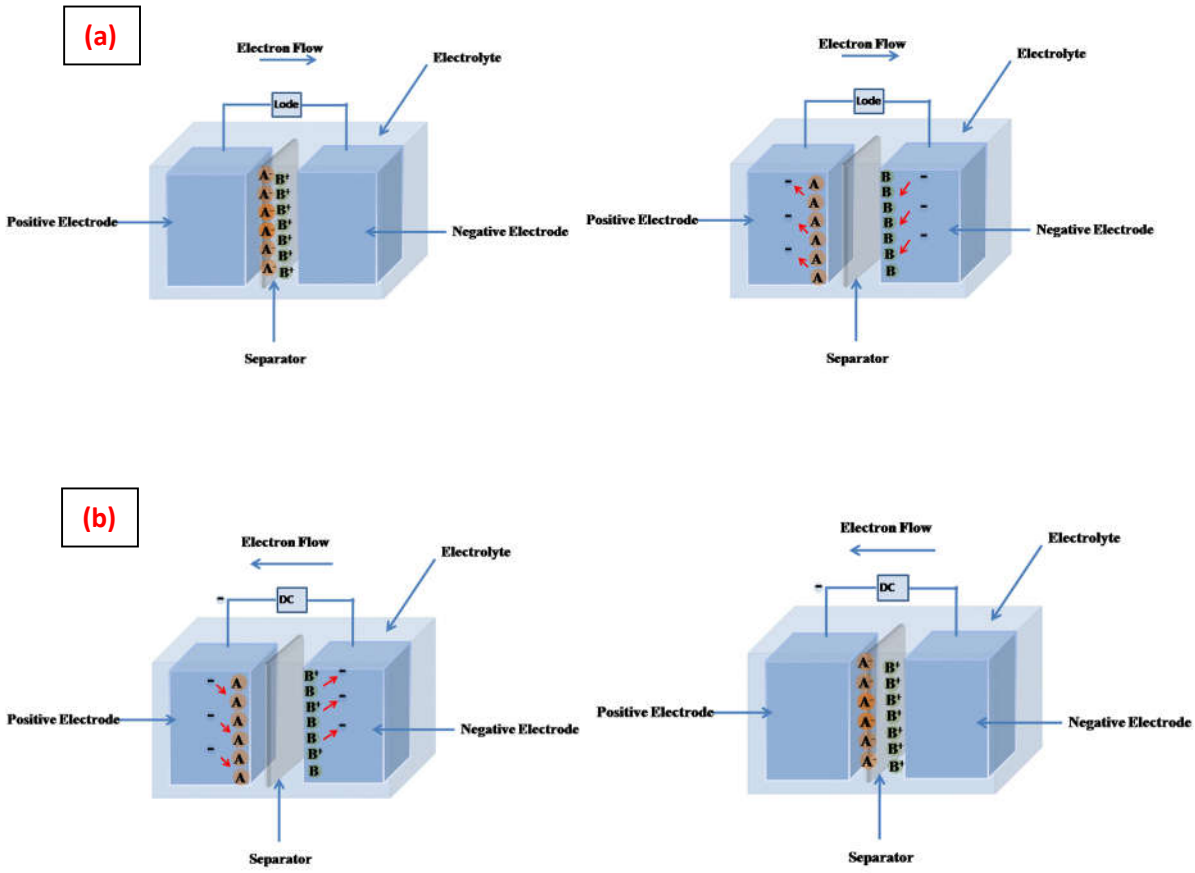

Figure 1.4: Schematic of Pseudocapacitors (a) charging (b) discharging.

Transition metal oxides, conducting polymers and mixed transition metal oxides have been widely studied as an electrode material for pseudocapacitors.

Transition metals oxides are promising electrode material because they can store energy in the faradic and non-faradic way hence have very high specific capacitance.[5] Metal oxides like ruthenium oxide, manganese oxide, cobalt oxide, vanadium oxide, nickel oxide have been widely studied. Ruthenium oxide attains high attention due to its high specific capacitance, reversibility, and conductivity. The high cost of noble metal ruthenium hinders it for commercial production. Various electrochemical studies in these

metal oxides have been done by changing the morphology and porosity. The protons can freely intercalate and de-intercalate into the metal oxide lattice and facilitate oxidation-reduction reaction easily.

Mixed Transition Metal Oxides (MTMO) are another group of interesting materials which have excellent electrochemical properties for supercapacitor application.[5] Mixed transition metal oxides such as $NiCo_2O_4$, $ZnCo_2O_4$, $MnCo_2O_4$, $CoMoO_4$, $CuCo_2O_4$, $MnMoO_4$, $NiMoO_4$, $CuFe_2O_4$ are widely studied as an electrode material. $NiCo_2O_4$ is most promising MTMO which have a very high specific capacitance, high electrical conductivity, long cycle life and low cost compared to other mixed transition metal oxides.[1-5] Its pseudo-capacitance behavior in alkaline medium can be expressed as follow: [10]

$$\mathbf{NiCo_2O_4 + OH^- + H_2O \rightleftharpoons NiOOH + 2CoOOH + e^-}$$

$$\mathbf{CoOOH + OH^- \rightleftharpoons CoO_2 + H_2O + e^-}$$

$NiCo_2O_4$ have been widely studied as electrode material by changing its morphology in nano region as nanorods, nanospheres, nanoflowers, urchin-like, pine-like, core-shell structure etc.[1-9] Nickel cobalt oxide have shown a high capacitance of 3.51F/cm^2 at a current rate of 1.8mA/cm^2.[3] The effect of change in capacitance with respect to change in morphology have been widely studied. There are few studies which talk about the pore size and surface area relation to the increase in capacitance. Many recent studies have focused on change in capacitance with a change in conducting substrate like nickel foam, Carbon cloth, titanium foam and so on. Some studies focused on hybrid materials like Nickel cobalt oxide on top of carbon nanotubes, graphene oxide and other metal oxides. But most of these studies do not discuss the basic electrochemical properties of the materials like electrochemical active surface area, Leakage current, Self-discharge, change in oxidation and reduction potentials. Self-discharging and leakage current measurements have a very important place in supercapacitor application to understand the efficiency of the supercapacitor to store charge for longer time.

In this work, we study the change in electrochemical properties on mixed transition metal oxides by controlled synthesis of the hierarchical nanostructures directly on metallic substrate and study the effect of site exposed cations in different morphologies. This project starts with the modified hydrothermal synthetic technique to synthesize nanocrystalline nickel cobalt oxide in pure spinel phase with different morphologies. The properties of the hierarchical nanostructures suitable for supercapacitor applications were tailored by systematic variation in reaction conditions and supersaturation level of the reaction mixture. We have observed a change in electrochemical properties (oxidation and reduction potentials) with a change in morphologies. As the use of binders in the drop-casting technique can hinder the accessibility of the material by ions, we have fabricated binder-free electrodes by growing nickel cobalt oxides directly on nickel foam. Instead of using the surface area from the BET measurement we have used electrochemical active surface area from double layer capacitance in order to account for the surface which is only in contact with the electrolyte.[13,14] The electrochemically active surface area is used to normalize the electrochemical properties instead of normalizing by geometrical area or mass of the electrode material. Present study also focuses on investigating the supercapacitive failure mechanism by leakage current and self-discharge rate of different morphologies of nickel cobalt oxides.

CHAPTER 2

In this chapter, we have discussed the synthetic protocols, structural and electrochemical characterization tools and techniques used to characterize the materials. The chapter starts with synthesis procedure and different optimization conditions to tailor the morphology. It also describes the methods in which the electrodes are fabricated. We have briefly discussed the theory behind X-ray diffraction, field emission scanning electron microscope (FESEM), thermogravimetric analysis and electrochemical workstation.

2. Experimental

2.1. Materials Synthesis

Synthesis of spinel $NiCo_2O_4$ nanostructure was done by a modified synthetic route of simple hydrothermal method followed by annealing.[19-23] 0.05M and 0.1 M respectively of nickel chloride hexahydrate, cobalt chloride hexahydrate were mixed with urea in the molar ratio of 1:2:2, 1:2:20, 1:2:30, 1:2:40. The homogeneous mixture was then transferred to a Teflon lined stainless steel autoclave and kept in a preheated electric oven at 180^oC for 12 hr. The brown precipitate was washed and centrifuged with water, ethanol for several time and dried at 115^oC in an air atmosphere for 12 hr. The precursor obtained was annealed at 350^oC for 3hr in an air atmosphere with a heating rate of 2^oC/min to obtain nickel cobalt oxide. The samples were named as I-rod, II-Urchin, III-mixed and IV-platelet respectively for 1:2:2, 1:2:20, 1:2:30, 1:2:40 molar ratio precursors. For synthesizing nickel cobaltite on nickel foam we kept cleaned nickel foam in the teflon container before the hydrothermal process. Cleaning of Nickel foam for removing the oxide layer was done by ultra-sonicating it in 3M HCl, water and ethanol for 30min.

2.2. Electrode Preparation and Measurements

Electrochemical studies of $NiCo_2O_4$ nanostructures of different morphologies were performed on an electrochemical workstation. Cyclic voltammetry (CV) in different scan rate and galvanostatic charging-discharging at various current densities are taken for different morphologies. This study was carried out with three electrode system in 3M KOH solution. Pt foil and Hg/HgO electrode were used as counter and reference electrode respectively. The working electrode is prepared by mixing active material, super P (conducting material) and PTFE (binder) in a ratio of 80:15:5 with IPA to obtain a consistent slurry. This slurry was drop coated on 3mm glassy carbon electrode. All the measurements are taken after a constant purging of nitrogen gas to remove dissolved oxygen from the electrolyte.

We fabricated a binder-free electrode method by directly aligning and growing the $NiCo_2O_4$ nanostructures on top of nickel foam. A 1cm x 1cm electrode is fabricated and used as a working electrode instead of a glassy carbon electrode.

2.3. X-Ray Diffraction

The X-Ray diffraction technique is used to study the crystallographic properties of the sample. Interaction of X-ray with the crystallographic planes can give information about the crystallographic phase of the sample, crystallite size, lattice parameters, strain and preferred growth direction. The constructive interference of X-rays when it diffract through the planes of crystals obeys Braggs law,

$$n\lambda = 2d\sin(\theta)$$

where‘ λ’ is the wavelength of incident X-ray

‘d’ is the interplanar distance

‘Θ’ is the angle of diffraction

‘n’ is the order of diffraction.

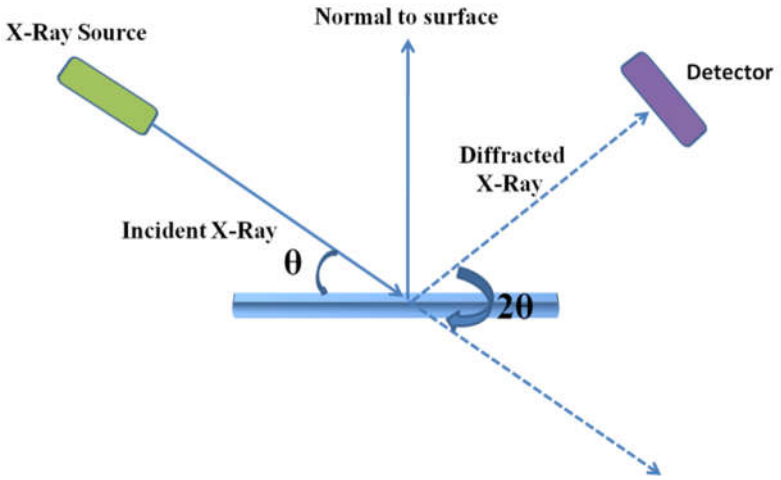

Figure 2.1: Schematic representation of X-ray diffractometer

X-Ray diffractometer mainly consists of an X-Ray source, sample holder and X-Ray detector. X-Rays are generated by the bombardment of high-velocity electrons produced by an electron gun onto a substrate like copper. If the energy of an electron is sufficient to dislocate the electron from the inner shell of the substrate, X-Rays are generated. The generated X-Rays are filtered by a monochromatic filter and bombarded on the sample. The diffracted X-Rays are collected by X-Ray detectors at various angles and intensity is recorded.

2.4. Field Emission Scanning Electron Microscope – FESEM

Field emission scanning electron microscope (FESEM) is used to study the morphology of conducting samples. Electron beams which are produced through field emission are focused and directed by magnetic lens and anode respectively. These electrons interact with the sample and produce both secondary and backscattered electrons. Secondary electrons are produced when the incident electron beam excites the sample and emits low energy electrons from its surface. Backscattered electrons are produced when an incident electron gets reflected back by the sample. Detectors are kept closer to the walls for secondary electrons and it is kept nearby the electron beam for backscattered electrons.[18]

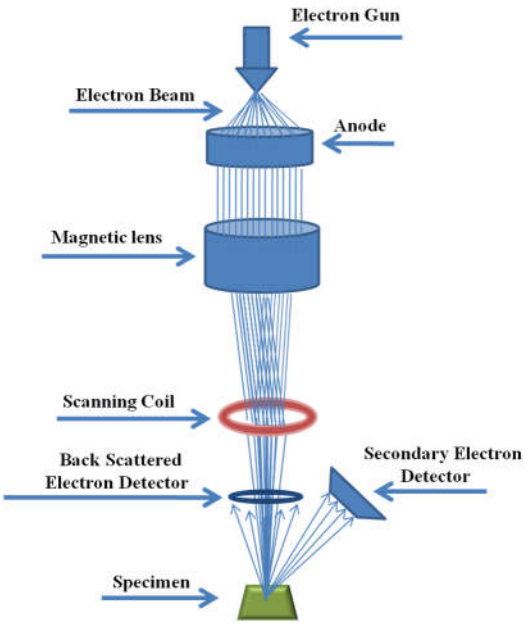

Figure 2.2: Schematic representation of FESEM

2.5. Thermogravimetric analysis (TGA)

Thermogravimetric analysis is the study of change in physical or chemical properties of a material with respect to change in temperature or time. We can study the decomposition, evaporation, reduction, desorption, oxidation and absorption by analyzing the weight loss or gain by the sample in time and change in temperature. In the present study, a dynamic thermogravimetric technique is used where the mass change is measured with a linear change in temperature. This technique is used to understand the decomposition and thermal stability of our material and to determine the right annealing temperature for further studies.

2.6. Electrochemical Workstation

Cyclic Voltammetry

In a cyclic voltammetry, a potentiostat will control a constant change in potential difference between the counter electrode and the working electrode and measure the change in current between the same.

Galvanostatic Charge-Discharging.

In galvanostatic charge-discharging, a constant current is measured and change in potential with respect to time is measured.

Theory and Calculations

The **specific capacitance** of each sample was calculated from galvanostatic charge - discharge by the equation,

$C = (I \times \Delta t) / V(1)$

I - constant current density in A/g.

Δt - time is taken for complete discharge in seconds.

V - potential difference in Voltage.

Specific energy is calculated by the equation,

$$E = C \times \Delta V^2 / 2$$ - Symmetric Capacitors (2)

$$E = C \times \Delta V^2 / 8$$ - Symmetric Capacitors using 3 electrode system (3)

Specific Power is calculated by the equation,

$$P = E / \Delta t \quad (4)$$

Electrochemical active surface area is measured from the double layer capacitance.[13,14,24]

$$I = (dQ/dt)$$

$$I = (dQ/dE) \times (dE/dt)$$

$$I = C \times v \quad (5)$$

CHAPTER 3

Results and Discussion

In the present proposed project work, we used a modified one-pot hydrothermal route to systematically tailor the morphology of the electrochemically active $NiCo_2O_4$ hierarchal architectures simply by changing the molar ratio of the metal cations to the stabilizing agent. The structural and electrochemical properties were studied by a multi-technique approach that includes powder X-ray diffraction (PXRD), field emission scanning electron microscopy (FESEM), thermogravimetric analysis (TGA), BET surface area measurements, cyclic voltammetry (CV), galvanostatic charge – discharging (GCD), Self-discharging, Leakage current measurements. We developed a robust strategy to grow $NiCo_2O_4$ nanocrystals of different morphologies directly on Ni foam. The suitability and the limitations of various morphologies were studied and compared for their potential supercapacitance applications.

3.1. Structural and Morphological Characterization

The as-prepared precursors obtained after hydrothermal treatment were first analyzed by thermogravimetric analysis (TGA) in order to understand the thermal behavior and to determine the follow-up calcination temperature. Figure 3.1 show characteristic TGA plot of the $NiCo_2O_4$ as-prepared precursors of I-rod and II-urchin samples. This clearly indicated major weight loss of ~30% occurred at offset temperature of 350°C and the decomposition temperature matches well with the earlier report. TGA analysis of the as-prepared samples clearly reveals that 350°C is an appropriate temperature for further annealing of the precursor which is likely to give crystalline phase of homogeneous $NiCo_2O_4$ phase. The annealed as-prepared samples were further characterized for phase purity by powder X-ray diffraction patterns.

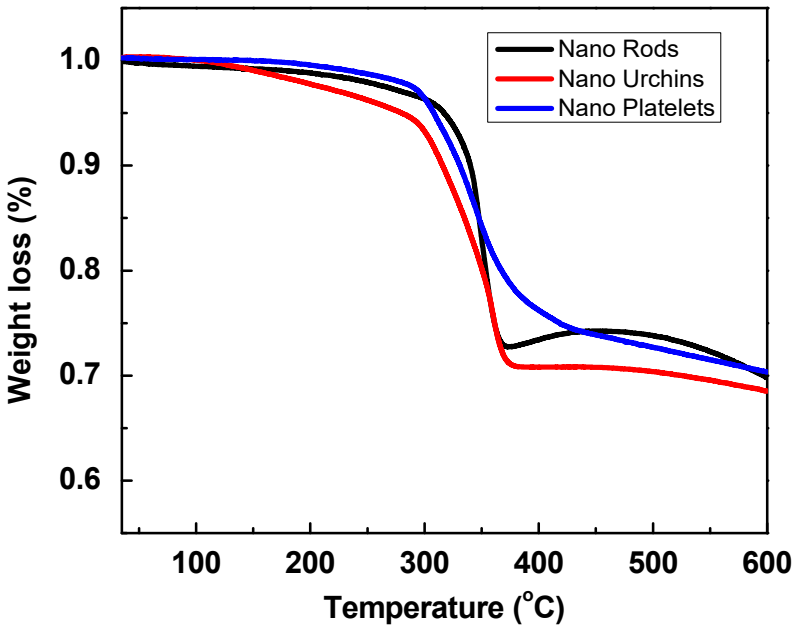

Figure 3.1: Thermogravimetric curves of $NiCo_2O_4$ nanocrystals of different morphologies

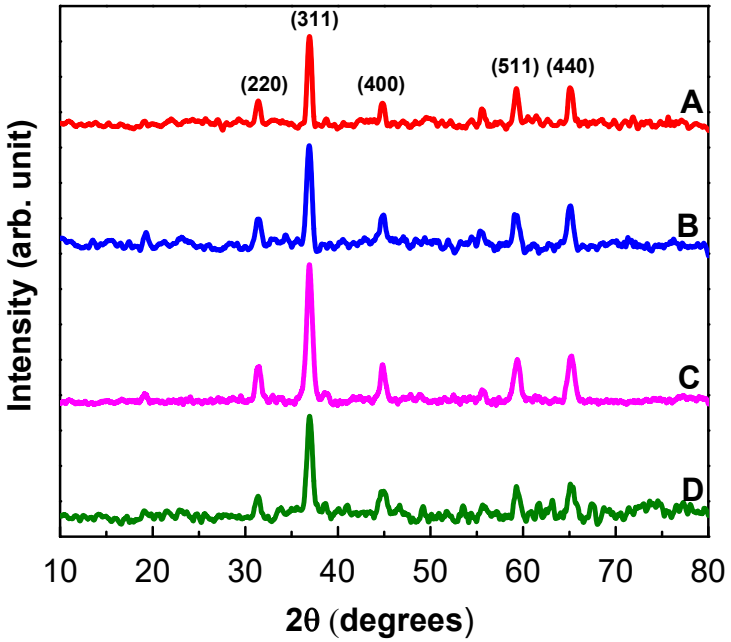

Figure 3.2: XRD patterns of (A) I-rods (B) II-urchin (C) III-mixed (D) IV-platelets $NiCo_2O_4$ nanoparticles

Figure 3.2 shows the powder X-ray diffraction patterns of $NiCo_2O_4$ nanocrystals of different morphologies, obtained after annealing the samples at 350°C. The XRD peak positions and the relative intensity of all reflection corroborate well with the standard pattern (JCPDS card no. 20-0781), clearly indicating the formation of a homogeneous spinel phase. The lattice parameter values calculated for these samples were slightly higher (8.12-8.14 Å) than the value reported for the bulk samples (8.11Å) and the effect is attributed to the nanocrystalline nature of the particles formed. The average crystallite sizes were derived using Scherrer's equation, $d = (0.9\lambda/\beta \cos\theta)$, where d is the diameter in angstroms, β is the half-maximum linewidth, and λ is the wavelength of X-rays. The average crystallite sizes for the samples annealed at 350°C was found to be in the range of 13nm to 16nm (±1) nm. On further annealing at 550°C, additional reflections corresponding to NiO phase appears which is about 15-20% nominally based upon the relative intensity (see Figure 3.3). This is due to the partial decomposition of spinel phase which is accompanied by the formation of cobalt-rich off-stoichiometric $NiCo_2O_4$ nanocrystals. The lattice parameter calculated for this sample is 8.10 Å which is slightly smaller than that reported for the stoichiometric samples.[25]This elucidates the presence of lattice distortion from the ideal spinel structure and much detailed work on off-stoichiometric $NiCo_2O_4$ nanocrystals has been reported earlier by our group.[25]

From Scherrer equation, the average crystallite sizes of the samples were found to increase from 16 (±1) nm to 37(±1) nm after annealing at 550°C. A systematic growth of the particles on annealing is attributed to the diffusion mechanism.

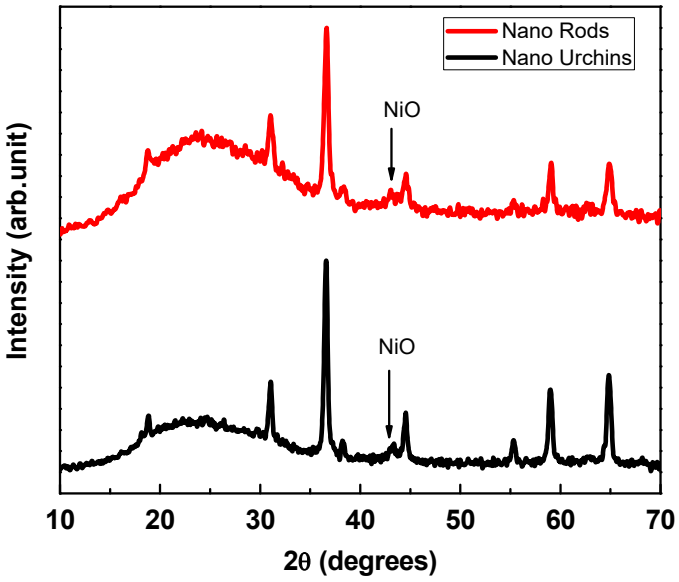

Figure 3.3: XRD patterns of nickel cobalt oxide Nano l-rods and Nano urchins obtained after annealing at 550°C.

Detailed structural and morphological studies were performed utilizing low and high magnification field emission scanning electron microscopy (FESEM) images. Figures 3.4 and 3.5 show the morphology of nickel cobaltite formed after annealing at 350°C. An analysis of the FESEM images clearly indicated the self-assembly of nanocrystals to form attractive mesoporous hierarchical nanostructures in which smaller nanocrystals self-assembled to form nanotube bundles and urchin structures. For the intermediate ratio of metal ion and urea, we could see the systematic assembly of nanotubes which sinters to form porous nanoplates. Such a mechanism seems to be a common phenomenon during crystal growth process and is observed for several material systems, such as carbonates, silicates etc. Indeed, detailed TEM studies and small angle X-ray scattering measurements are required to further elucidate these observations.

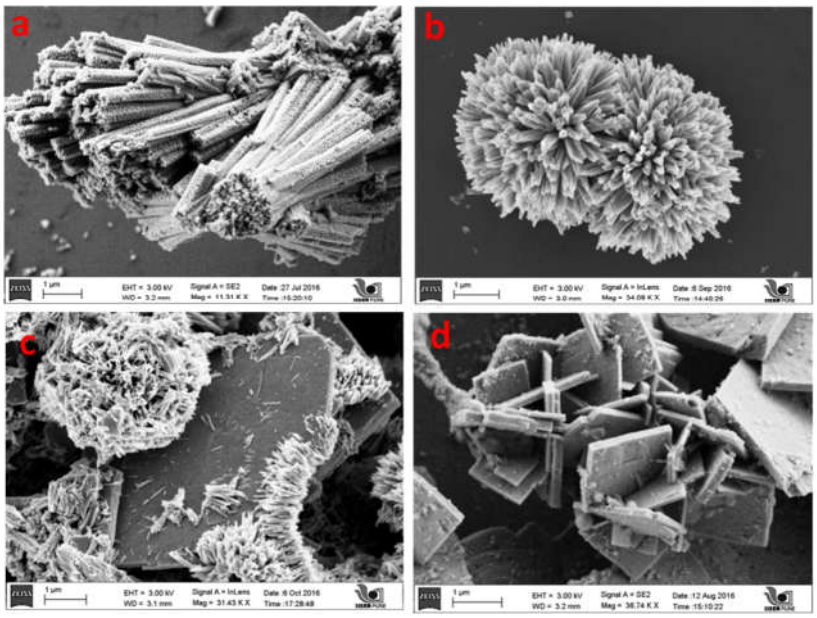

Figure 3.04: Low magnification FESEM image of (a) I-Rods, (b) II-Urchin, (c) III-mixed and (d) IV-Platelet $NiCo_2O_4$ nanocrystals.

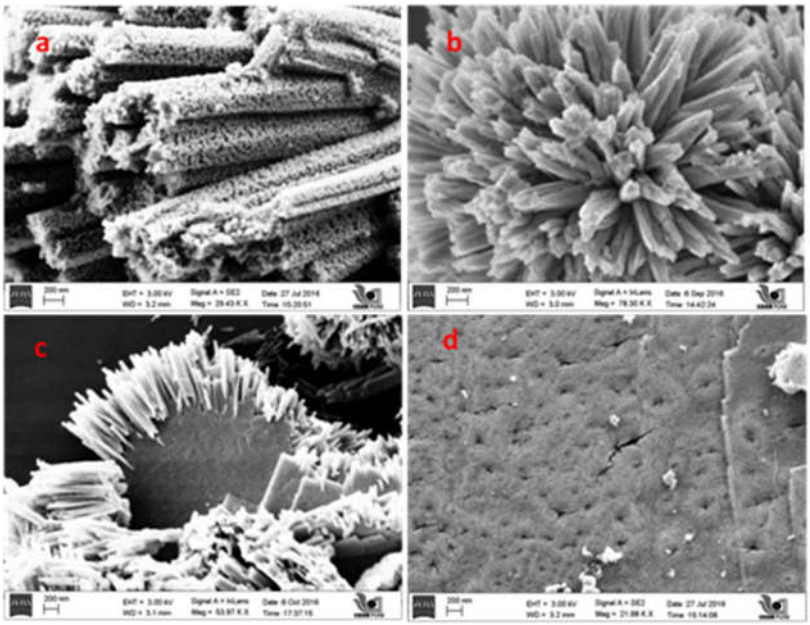

Figure 3.5: High magnification FESEM image of (a) I-Rods, (b) II-Urchin, (c) III-mixed and (d) IV-Platelet $NiCo_2O_4$ nanocrystals.

The specific surface area and hierarchical mesoporous nature of the I-rods and II-urchin $NiCo_2O_4$ nanostructures were further investigated by nitrogen adsorption-desorption measurements. The mesoporous structure was further supported by the Barrett-Joyner-

Halenda (BJH) pore size distribution and the Brunauer-Emmett-Teller (BET) surface area of I-rods and II-urchin $NiCo_2O_4$ nanostructures were calculated to be ~85 m^2/g and 135 m^2/g respectively confirming that these samples may be a potential candidate for electrochemical supercapacitor applications.

3.2. Electrochemical Analysis

Electrochemical properties of nickel cobalt oxide nanostructures were characterized mainly by cyclic voltammetry and galvanostatic charge-discharging. The oxidation-reduction potentials of the materials were determined by the CV studies. The specific capacitance of each sample was calculated from galvanostatic charge - discharge by the equation (1).

Figure 3.6 shows cyclic voltammetry (CV) analysis for samples at various scan rates in the potential window of 0 - 0.6 V. The shape of the CV curves clearly reveals the pseudocapacitive characteristic behavior with a distinct pair of redox peak corresponding to M-O to M-O-OH conversion. It can be seen that the anodic peaks shifts towards positive potential and cathodic peaks shift towards negative potential with the increase in the sweep rate. Interestingly, the position and intensity of redox peaks were significantly changed for each morphology clearly indicating the presence of different surface exposed cations. In order to further evaluate the application potential of the nanostructures of different morphologies, galvanostatic charge-discharging measurements were carried out in a 3 M KOH electrolyte at various current densities (see Figures 3.6: D, E and F).

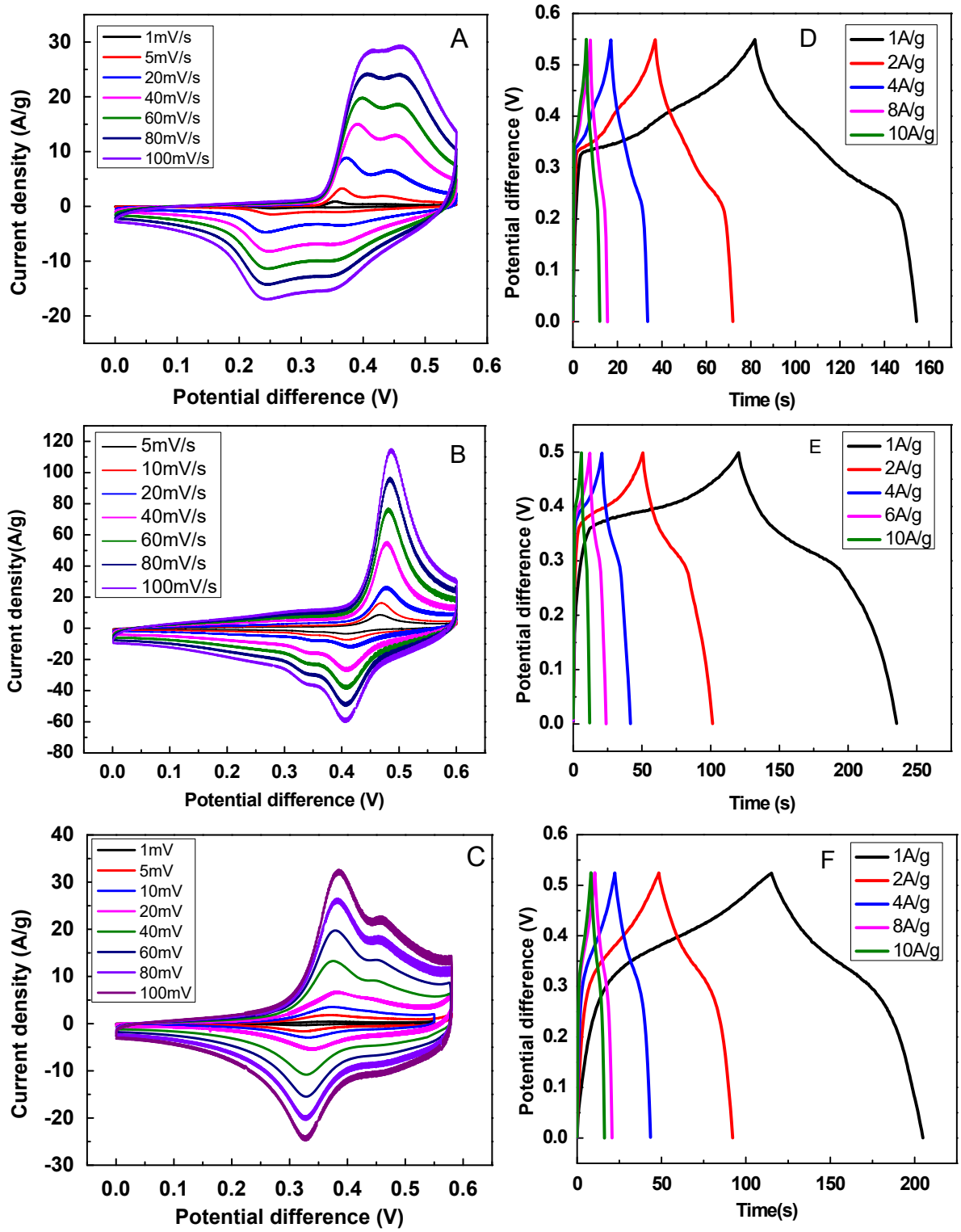

Figure 3.6: Comparative cyclic voltammetry (A, B and C) and corresponding charging-discharging profiles (D, E and F) for I-Rods, II-Urchin and III-mixed $NiCo_2O_4$ nanocrystals respectively.

The specific capacitance of nanorod bundle like urchin like and platelet-like structures at 1A/g was calculated to be 135 F/g, 240 F/g and 173 F/g respectively. Though we expected higher specific surface area owing to its superior morphologies and high surface area values, we could experimentally achieve lower values and found that the values were mainly governed by the way the electrodes were fabricated. In the case of dope-casting technique, we have to use a binder to get a stable and uniform coating on top of the working electrode. This polymer can cover a major portion of the electrochemically active surface area and decrease the capacitance to several folds. In order to get a structurally stable electrode without using binders, we have fabricated nickel cobalt oxide nanoparticles on top of nickel foam (current collector).

3.3. Binder free Electrodes

In order to get structurally stable and uniform working electrode, we utilized binder-free electrode fabrication method by directly aligning and growing the $NiCo_2O_4$ nanostructures on a conductive substrate such as Nickel foam by in-situ hydrothermal reactions.

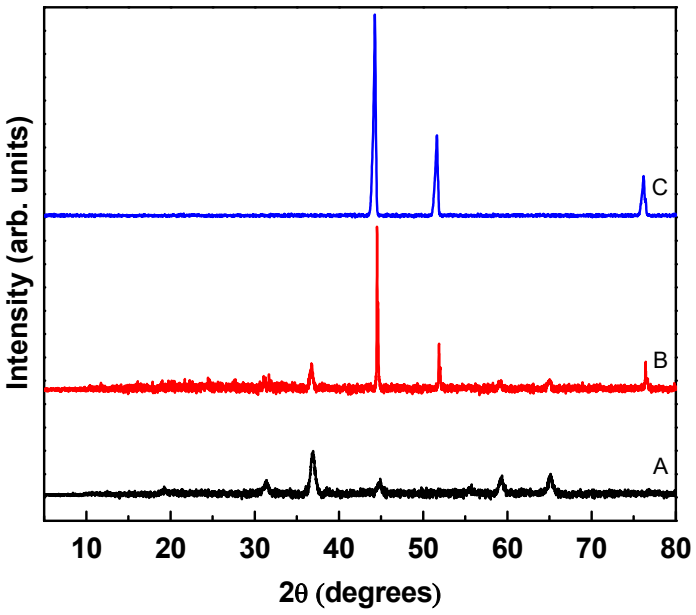

Figure 3.7:(A) Nickel cobalt oxide in urchin morphology,(B) Nickel Cobalt Oxide on Nickel foam (Needle-like) and (C) PXRD pattern of Nickel foam.

Figure 3.7 shows comparative PXRD patterns of nickel foam, nickel cobalt oxide on nickel foam and nickel cobalt oxide powder. The PXRD peak positions and the relative

peak intensity corroborates well with the standard pattern (JCPDS card no. 20-0781) clearly indicating the formation of a homogeneous spinel phase.

Structural and morphological studies were done by FESEM. It was interesting to note that electrodes of varying morphologies were obtained on nickel foam simply by systematically changing the molar ratio of metal to urea. With a lower concentration of urea, nanocrystals self - assembled to form long and thin porous nanochannels like architectures with an average length of 10 to 12 μm and a width of 50 to 200nm(see Figure 3.8 (a)). Interestingly, with a supersaturated solution of urea (1:2:40), the nanocrystals self-assembled to form porous platelet structure (see Figure 3.8: (d)). We have observed similar morphology for the samples obtained as powder form. This may be attributed to the combustion nature of urea at 350^{o}C (see Figure 3.1) which lead to the multipoint nucleation and sintering simultaneously. With the intermediate concentration of the urea, we observed a hybrid structure of very thin nanowires on top of nanosheets was observed (see Figure 3.8: c). Indeed, much work in this direction is required to elucidate this fact and understand the mechanism.

Figure 3.9 shows CV at various rate of change of potentials (1mV/s, 2mV/s, 5mV/s and 10mV/s) on a potential window of 0 to 0.6V and charge-discharging at constant current rate (1mA/s, 2mA/s, 4mA/s, 6mA/s, 8mA/s and 1mA/s) for different morphologies.The shape of the CV curves clearly reveals the pseudocapacitive characteristics with a distinct pair of redox peak corresponding to M-O to M-O-OH conversion. It can be seen that the anodic peaks shifts towards positive potential and cathodic peaks shift towards negative potential with the increase in the sweep rate as observed previously with template free nickel cobalt oxide.

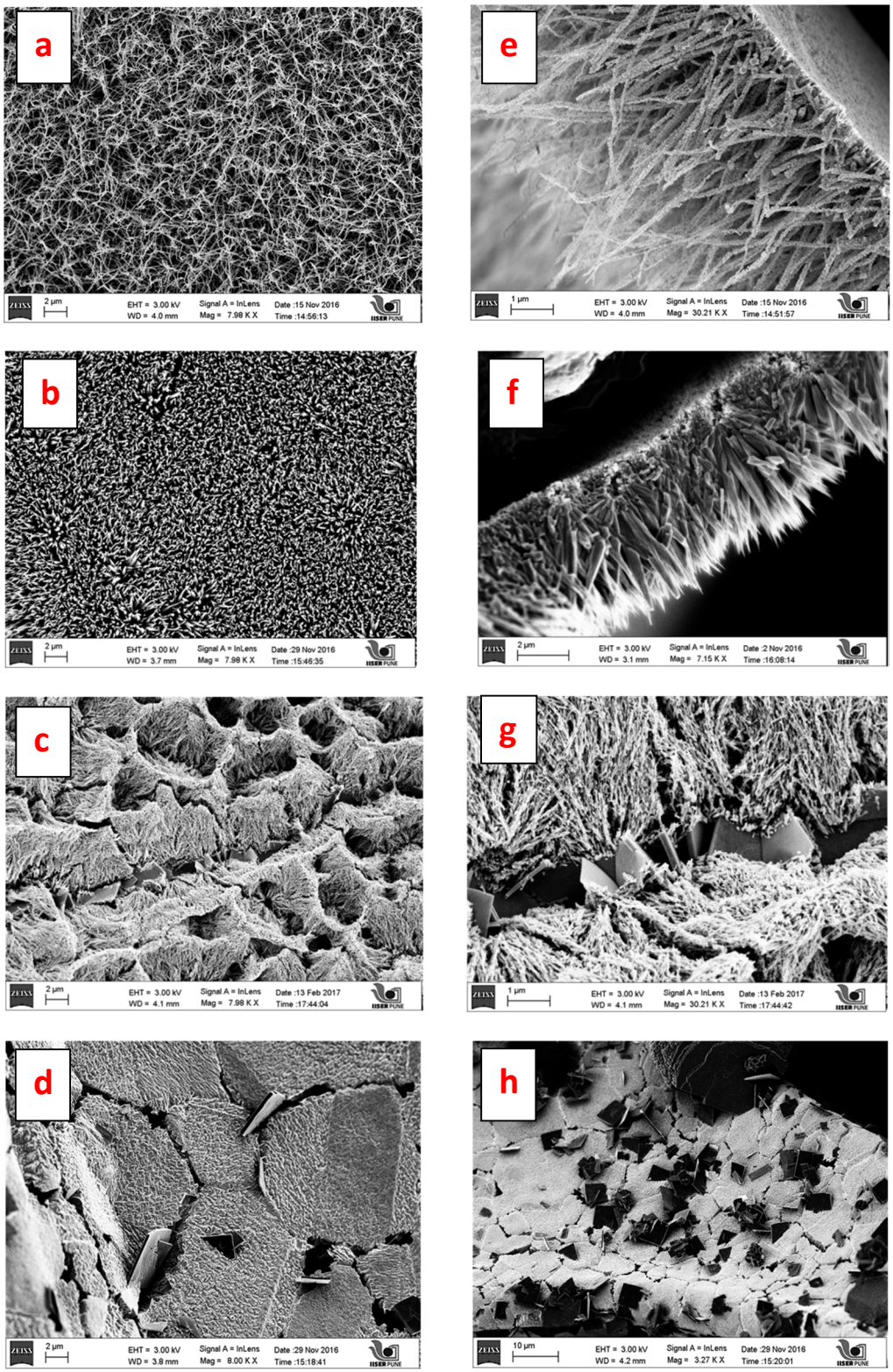

Figure 3.8 : FESEM of nickel cobalt oxide on nickel foam (a) Nano wires (b) Nano needles (c) Nano sheets with wires and (d) Platelet structure.Corresponding FESEM images at high magnification are shown in (e), (f), (g) and (h) respectively.

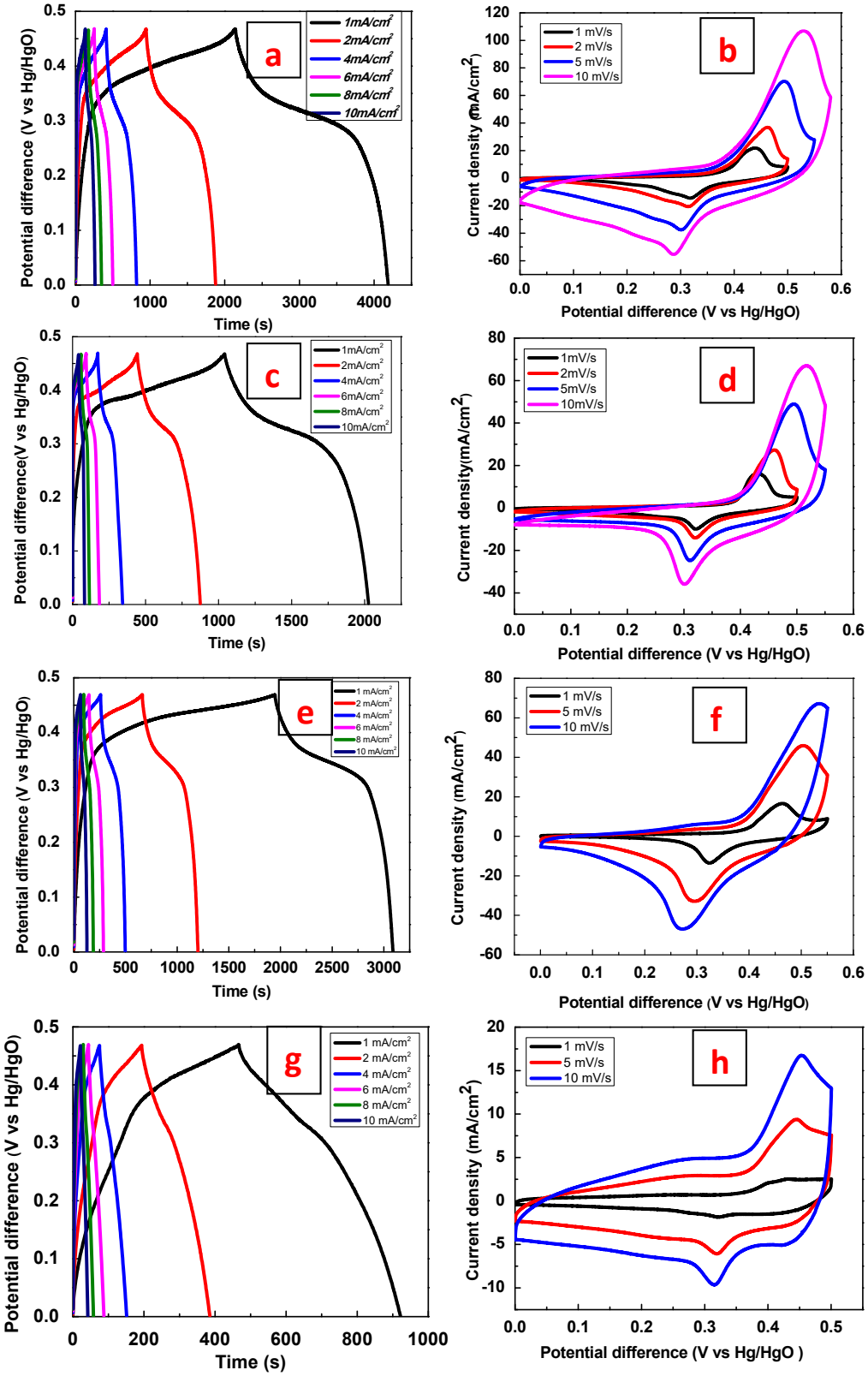

Figure 3.9 : Galvanostatic charge discharging and corresponding cyclic voltammetry of nanowires (a, b), Nanoneedles (c, d), Nanosheets with wires (e, f) and Platelet structure (g, h) nickel cobalt oxide respectively.

The specific capacitance of each morphology was calculated from galvanostatic charge-discharging. The nickel cobalt oxide nanowires were showing highest capacitance of 4349mF/cm^2 at a constant current rate of 1mA/cm^2. Our other values of the areal capacitance of 2445mF/cm^2, 2100mF/cm^2 and 968mF/cm^2 at a constant current rate of 1mA/cm^2 for nanosheets with nanowires, nanoneedles, and platelet structures respectively, clearly elucidate that the capacitance value is largely governed by the morphology of the electrode materials.

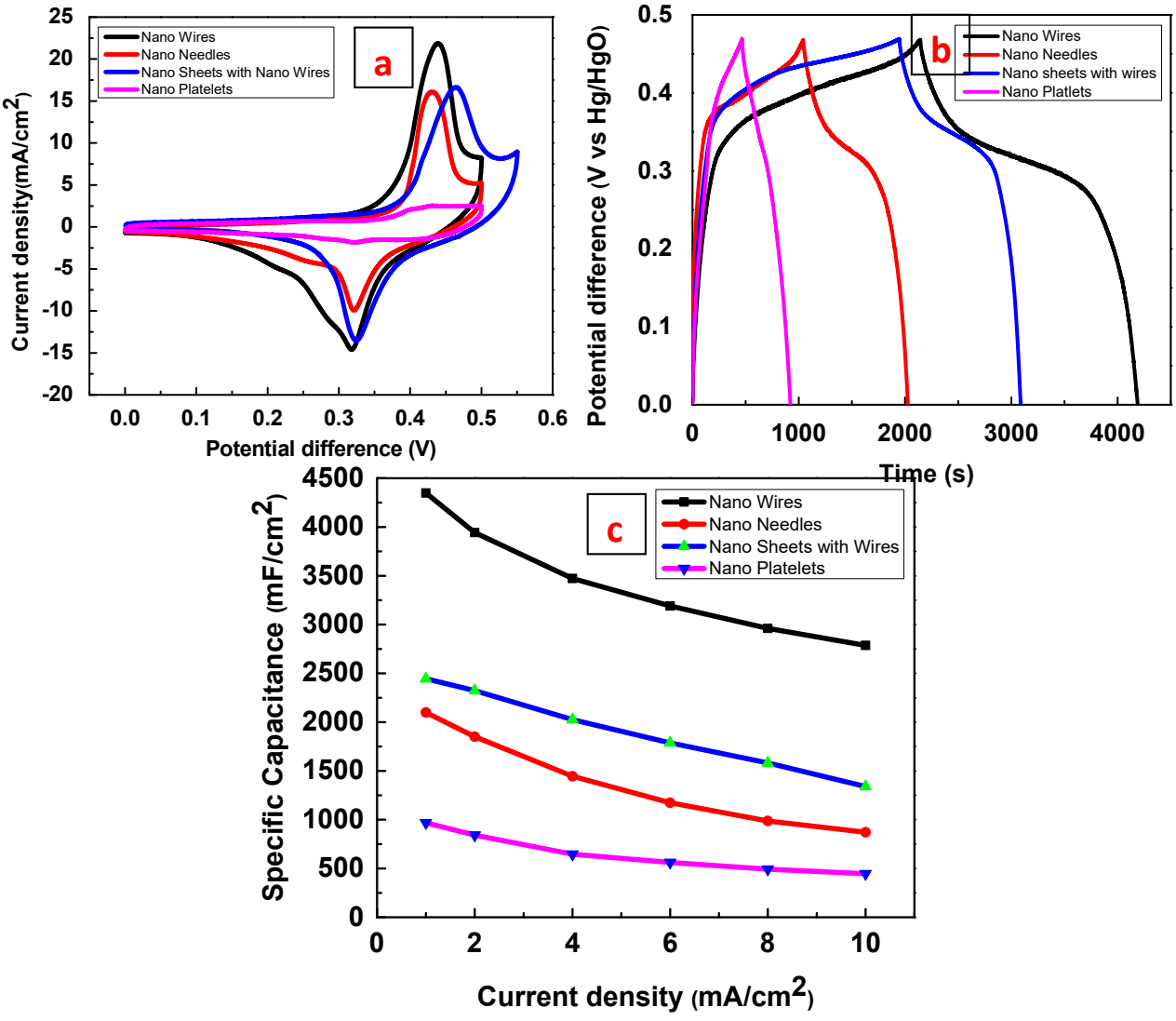

Figure 3.10: (a) Show Cyclic Voltammetry of Nickel cobalt oxide with different morphologies. (b) Galvanostatic charge-discharging of Nickel cobalt oxide with different morphologies. (c) Specific capacitance v/s current density for different morphologies.

Figure 3.10 (a,b) shows a comparative CV and Galvanostatic charge-discharging for different morphologies of nickel cobalt oxide. Figure 3.10 (c) shows specific capacitance with respect to change in current density in different morphologies. Nickel cobalt oxide nanowires show very high capacitance even at a high current density of 10mA/cm^2 as compared to other morphologies.

In order to understand the change in electrochemical properties of ternary transition metal oxide with binary transition metal oxides we have synthesized and studied nickel oxide and cobalt oxide materials with the identical conditions.

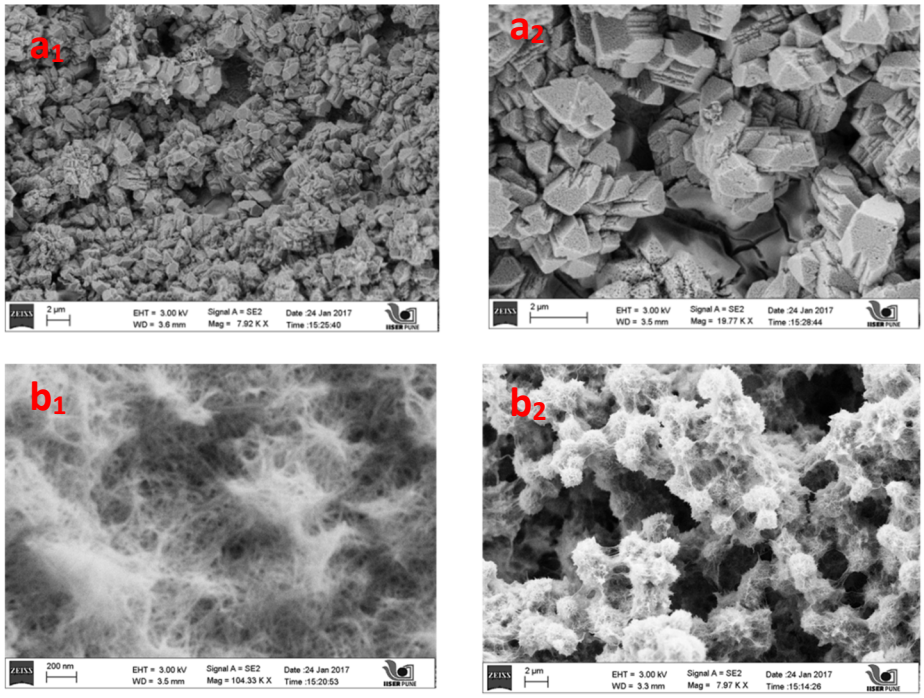

Figure 3.11: FESEM image of (a_1,a_2) Cobalt oxide (b_1,b_2) Nickel oxide

Figure 3.11 shows the FESEM images of nickel oxide and cobalt oxide. Cobalt oxide appears to form a brick like structures whereas nickel oxide forms a spherical structure constructed by very thin nanowires.

The CV and galvanostatic charge-discharging of nickel oxide and cobalt oxide at various scan rate and current density have been plotted in Figure 3.12. It is interesting to note that cobalt oxide show very high capacitance of 5508 mF/cm^2 at a current

density of 1mA/s whereas nickel oxide show a capacitance of 2977mF/cm^2 at a current density of 1mA/s. Since the amount of material deposited on top of nickel foam is different in each material, CV was normalized with respect to electrochemically active surface area in order to understand the reason behind this unexpected change in capacitance.

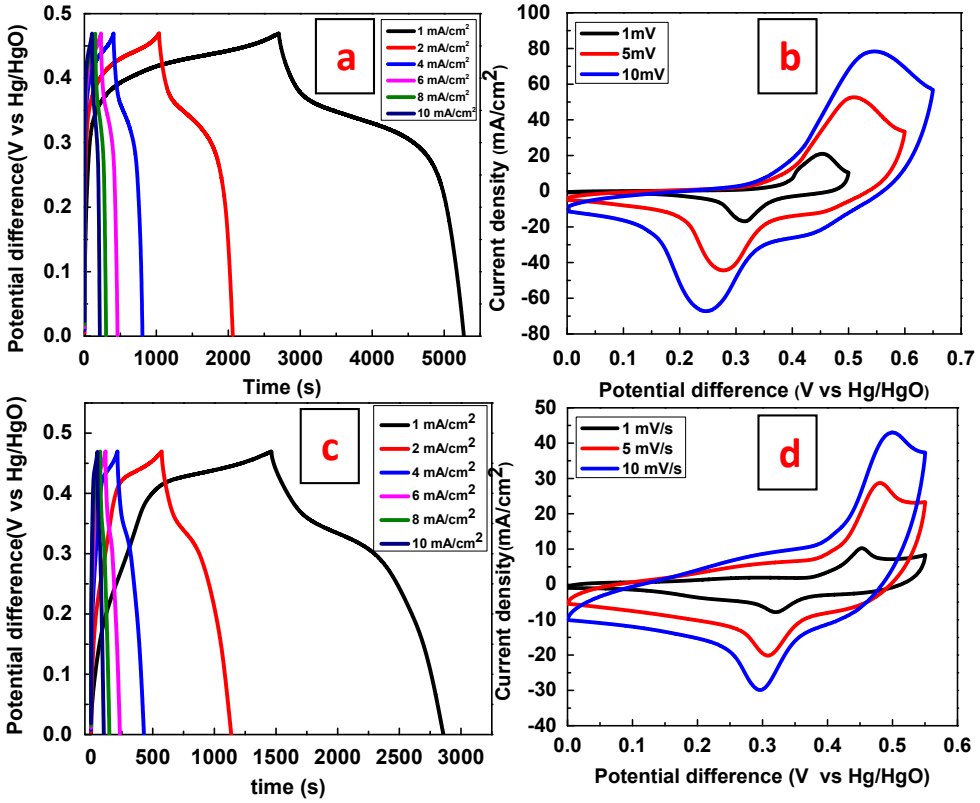

Figure 3.12: Galvanostatic charge discharging and CV of (a,b) Cobalt oxide (b,d) Nickel oxide.

Figure 3.13 (a) shows bar diagram of faradic efficiency and voltage efficiency of nickel cobalt oxide, cobalt oxide and nickel oxide at a current density of 1 mA/cm^2. Except for nickel cobalt oxide with nanosheets, all other materials show good faradic efficiency. Figure 3.13 (b) shows faradic efficiency and voltage efficiency of nickel cobalt oxide nanowires at different current density. Faradic efficiency increases with increasing current density whereas voltage efficiency decreases with increase in current density. Even at a high current density of 10mA/cm^2 voltage efficiency drop only by 12% compared to that of at 1mA/cm^2.

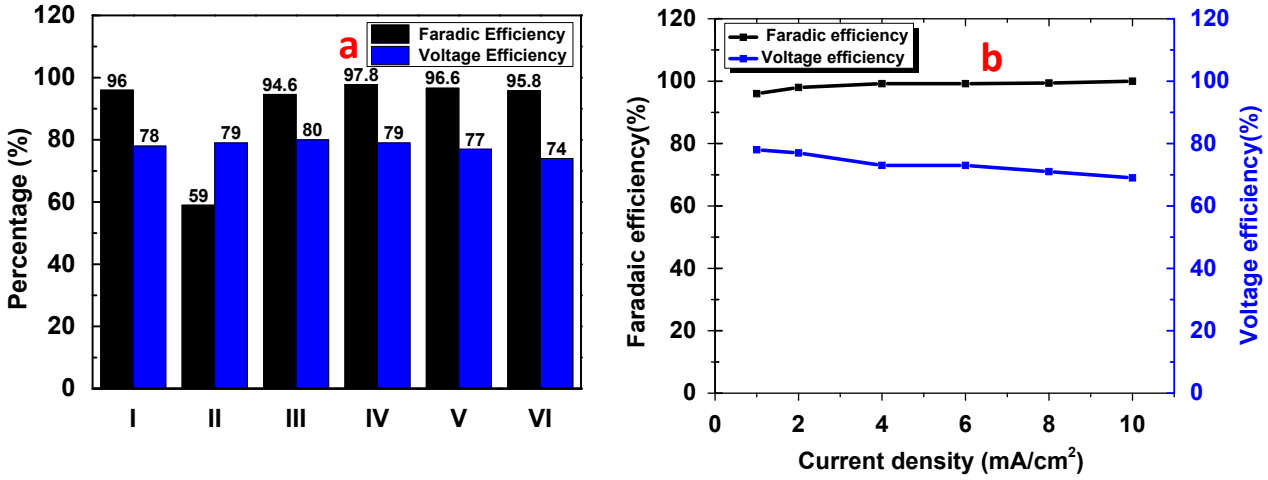

Figure 3.13: (a) Bar diagram representing Faradic efficiency and Voltage efficiency of Nickel cobalt oxide (I) nanowires ,(II) nanosheets with wires ,(III) nanoneedles ,(IV) platelets, (V) Cobalt oxide and (VI) Nickel oxide at a current density of 1mA/cm^2. (b) Faradic efficiency and Voltage efficiency of Nickel cobalt oxide nanowires at different current density.

3.4. Electrochemical Active Surface Area (EASA)

In order to understand the electrochemical material property without any surface area effect, we have to normalize CV with respect to its actual electrochemically active surface area. The electrochemically active surface area is measured from the double layer capacitance[13,14,24].

$$I = (dQ/dt)$$

$$I = (dQ/dE) \times (dE/dt)$$

$$I = C \times v \quad (5)$$

Where C is the capaitance in farad, v is the scan rate in V/s and I is the current in mA.

Double layer region has to be analyzed where the effect of faradic current is minimal. A potential window of 0 to 0.1V have been chosen and CV at different scan rate is recorded. Fig 3.14(a) shows the CV of different samples at the100mV/s.

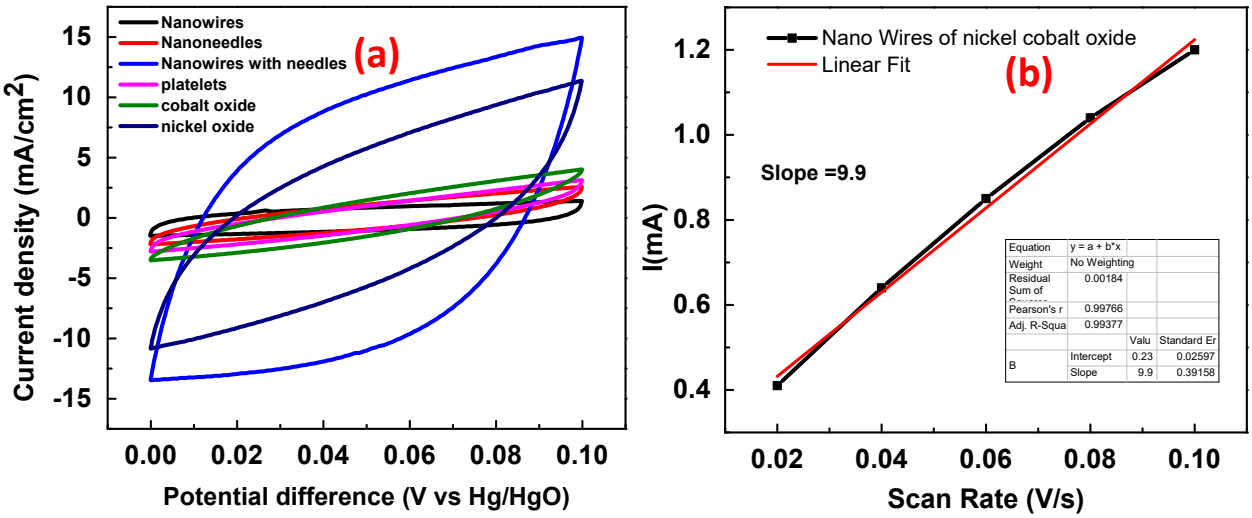

Figure 3.14: (a) CV of different morphologies of nickel cobalt oxide, cobalt oxide and nickel oxide at a scan rate of 100mV/s.(b) Liner fit of anode current with respect to scan rate for nickel cobalt oxide nanowires.

SI.No	Material	Double Layer Capacitance (mF)	Actual area (cm^2)	Capacitance (mF/cm^2) (geometrical area)	Specific Capacitance (mF/cm^2) (EASA)
1	Nickel cobalt oxide (Nanowires)	9.9	165	4349	26.4
2	Nickel cobalt oxide (Nanoneedles)	11.8	197	2100	10.66
3	Nickel cobalt oxide (Nanosheets with wires)	117.7	1961	2445	1.25
4	Nickel cobalt oxide (Platelet)	9.5	158	968	6.15
5	Cobalt oxide	18.45	307.5	5508	17.9
6	Nickel oxide	64.3	1071	2977	2.78

The normalized CV with different morphology and different material is plotted to understand the surface charge density of the material.

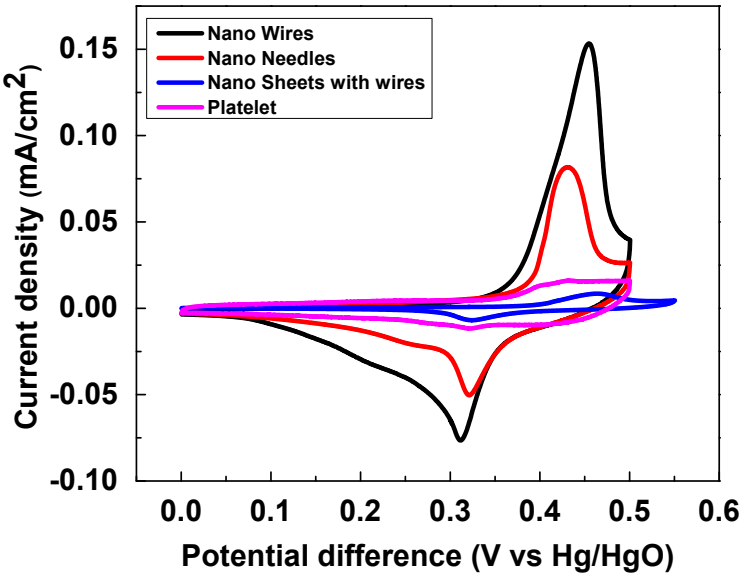

Figure 3.15: Normalized CV of Nickel Cobalt Oxide (a) Nanowires (b) Nanoneedles (c) Nanosheets with wires and (d) Platelets.

From Figure 3.15 we can understand a difference in surface charge density while changing the morphology of the Nickel cobalt oxide. Even though chemical compositions of all morphologies are identical and the surface area component is normalized, each morphology exhibits a drastic change in surface charge density. Nanowires are showing much higher surface charge density than any other morphology. This result strongly indicates the possibility of having different cation sites exposed to the surface in different morphologies.

From Figure 3.16 we can clearly see that the nickel cobalt oxide have much higher surface charge density than that of cobalt oxide and Nickel oxide. This proves our primary hypothesis of having binary metal oxide having lower surface charge density than that of ternary metal oxide.

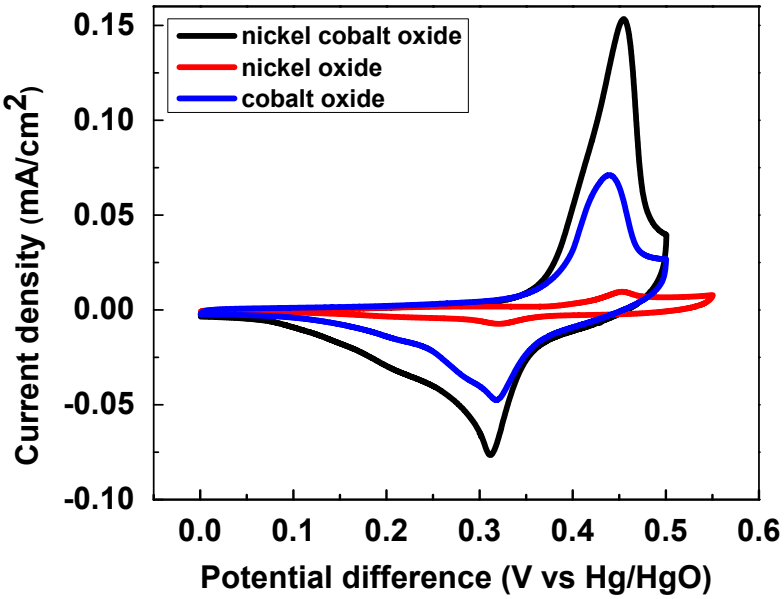

Figure 3.16: Normalized CV of (a) Nickel cobalt oxide (b) Nickel oxide and (c) Cobalt oxide

3.5. Symmetric Supercapacitor

We choose nickel cobalt oxide with nanowire morphology to check the performance in a two electrode symmetric system. Specific Capacitance of the system is derived from the equation 6.

$$C = 2 \times (I \times \Delta t) / (\Delta V \times A) \qquad (6)$$

C – Specific Capacitance

I – Constant Current density

Δt – Discharge time

ΔV – Potential Window

A – Geometrical area of electrode

Figure 3.17 shows the CV **(a)** and galvanostatic charge discharging **(b)** of two electrode symmetric system. Specific Capacitance as a function of current density is illustrated in **(c)**. Specific Capacitance of the system at a constant current density of 1mA/cm^2, 2mA/cm^2, 4 mA/cm^2,6 mA/cm^2 ,8 mA/cm^2 and 10 mA/cm^2 is 515mF/cm^2 , 370 mF/cm^2, 250 mF/cm^2,174 mF/cm^2, 120 mF/cm^{2}and 87.5 mF/cm^2 respectively.

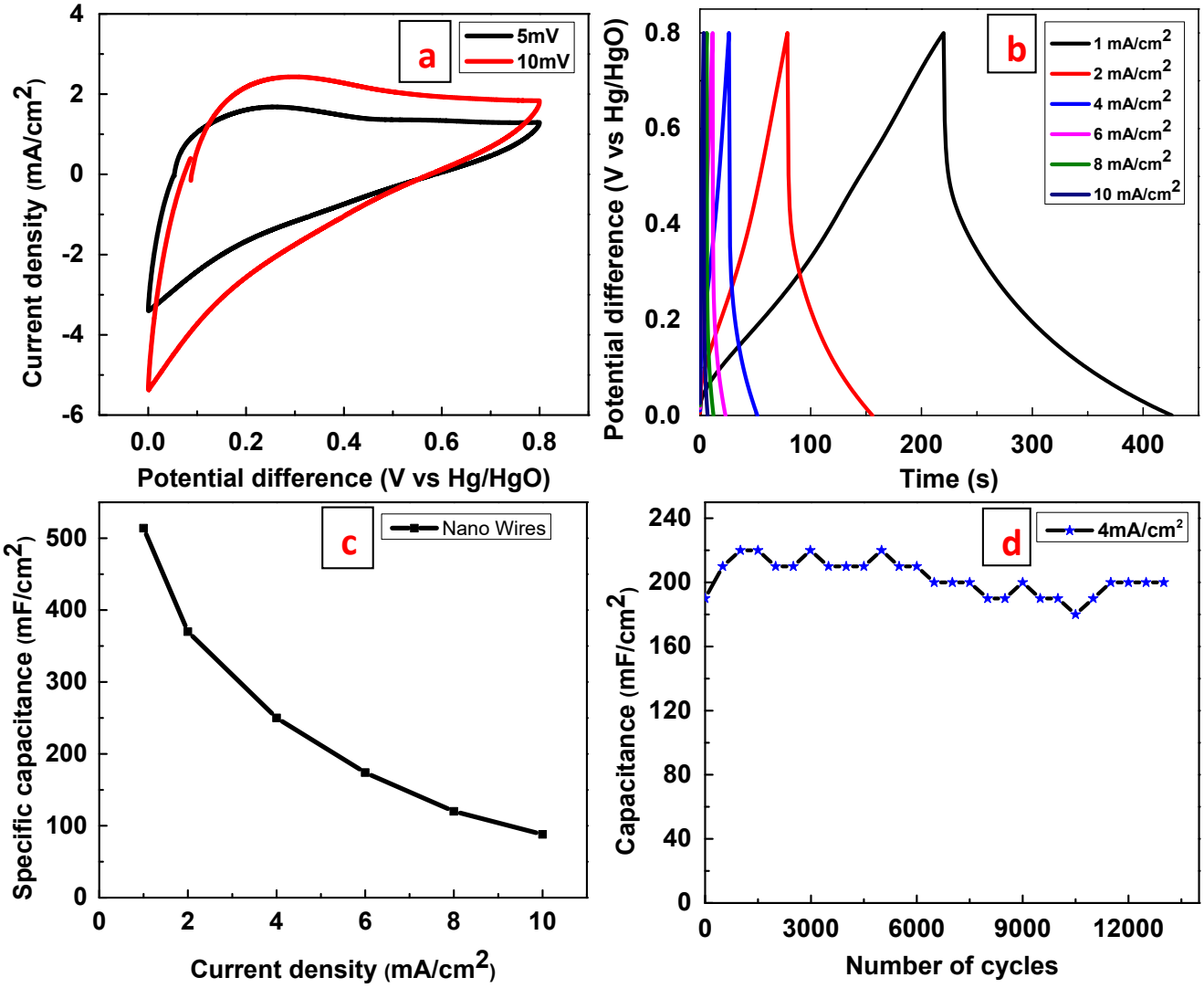

Figure 3.17: (a) Cyclic Voltammogram of nanowires of Nickel cobalt oxide at 5mV/s and 10mV/s. (b) Galvanostatic charge-discharging of Nickel cobalt oxide nanowires at different current density (1mA/cm^2,2mA/cm^2,4mA/cm^2,6mA/cm^2,8mA/cm^2,10mA/cm^2). (c) Specific capacitance as a function of current density. (d) Cycling performance at a high current density of 4mA/cm^2 over 13000 cycles.

The specific capacitance of this system is comparable to other literature values. There is a decrease in specific capacitance when the current density of charging and discharging the system increase. In order understand the stability of the electrode we have done the cycling stability measurements. Galvanostatic charge-discharge cycles at 4mA/cm^2 current density using nickel cobaltite nanowires demonstrated extended cyclability with more than 90% capacity retention at the end of 13000 cycles.

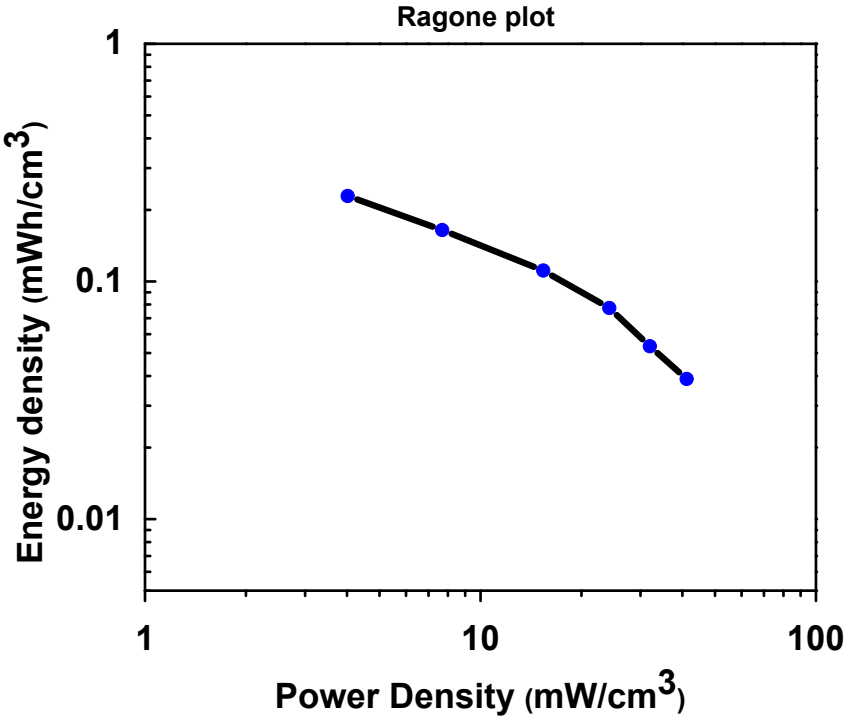

Figure 3.18:Ragone plot of nickel cobalt oxide nanowires at different current densities.

Ragone plot is one of the most important plots to analyze any energy storage device where X axis represents the specific power and Y axis represents the specific energy. Figure 3.18 represents the Ragone plot of the symmetric capacitor of Nickel cobalt oxide nanowires. X and Y axis is represented in logarithmic units for simplification. Energy and power of the device were normalized with respect to its device volume. Nickel cobalt oxide nanowires show a high energy density of 0.23mWh/cm^3 at a power density of 4mW/cm^{3}and a high power density of 41.2mW/cm^3 at an energy density of 0.04mWh/cm^3.These values are comparable to that of other literature. [6,25]

3.6. Self-discharging (SD) and leakage current (LC)

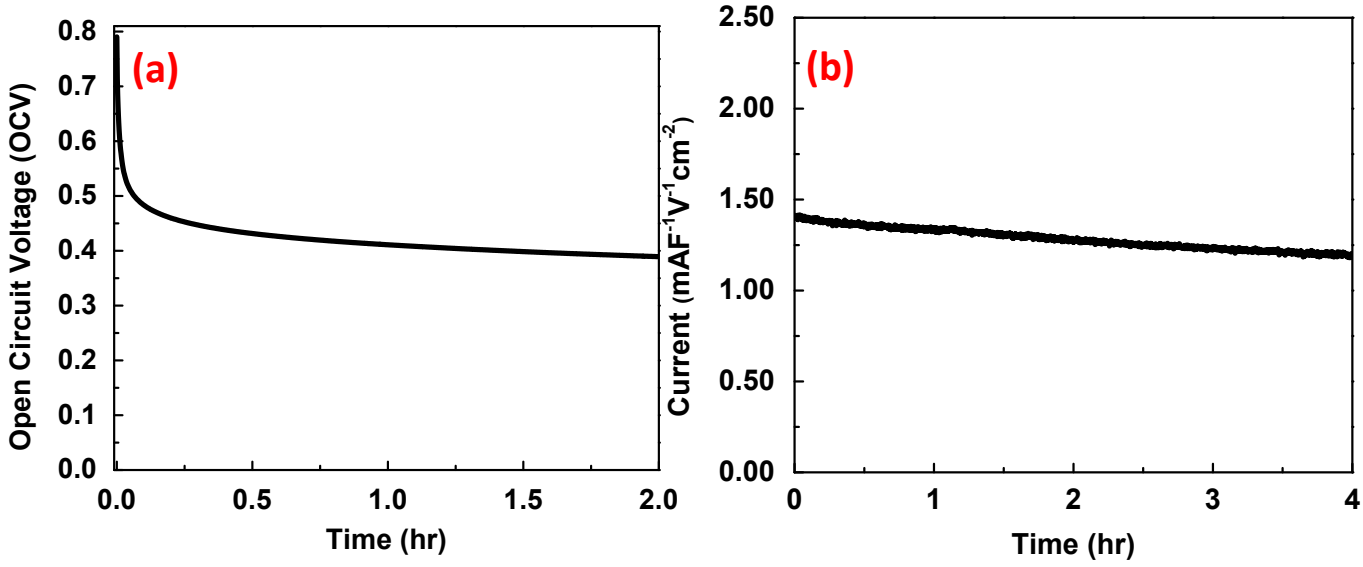

Figure 3.19: (a) Self-discharging of Nickel cobalt oxide nanowires. (b) The leakage current of Nickel cobalt oxide nanowires.

Self-discharge is the voltage drop experienced by the capacitor at a fully charged state. This measurement is very important for the device application. Compared to batteries supercapacitors have very high self-discharging properties.[12] In order to determine the self-discharging, the supercapacitor is charged to its full capacitance and holds the potential for 8hr at room temperature. Then we remove the bias and measure the open circuit voltage (OCV) between the electrodes. There is a steep decrease in the potential at the initial stage and then the potential get saturated. Figure 3.19 (a) shows the self-discharging property of Nickel cobalt oxide nanowires. The potential drop to its half of the initial potential takes more than 5000 sec which is a moderate value to the best of my knowledge. The self-discharging property is also dependent on the temperature at which it is measured.

At a fully charged state, the potential of the electrodes will be much higher than that of the OCV of the electrodes. The system will try to relax from this high energy state to a lower energy state if possible. There are mainly three reasons for self-discharging, self-

discharging due to ohmic leakage between the electrodes, faradic reactions and redistribution of charge from surface to bulk.[12]

Leakage current is defined as the current needed to maintain the capacitor as fully charged. Lower the leakage current, better the capacitor. Leakage current is measured just after keeping the capacitor fully charged for 4hr. Figure 3.19 (b) shows the leakage current measurement for nickel cobalt oxide nanowires. A moderate leakage current of 1.4 $mAF^{-1}V^{-1}cm^{-2}$ was obtained for nickel cobalt oxide nanowires.

Conclusions

The effect of pseudocapacitive charge injection/ejection in different morphologies of nickel cobalt oxide was studied in this project. Nickel cobalt oxide with different morphologies has been synthesized by changing the metal to urea ratio. Synthesis is optimized by controlling various parameters like time, concentration, and temperature. In order to achieve higher capacitance and stability, binder-free nickel cobalt oxide was grown directly on Ni foam. Morphologies like nanowires, nanoneedles, nanosheets with nanowires and platelet structures were obtained simply adjusting the metal to urea ratio. An extremely high capacitance value of 4349$mF/cm^2$is obtained for nickel cobalt oxide nanowires compared to other morphologies such as nanoneedles (2100 mF/cm^2), nanosheets with wires (2445 mF/cm^2) and platelets (968 mF/cm^2).To rule out the possibility of amplified surface area towards the extremely high areal capacitance of nickel cobaltite nanowires we have normalized the capacitance by the electrochemically active area. The resulting true area normalized capacitance values are noticeably higher (26.4mF/cm^2) in favor of nickel cobaltite nanowires compared to other morphologies and individual counterparts such as nickel oxide (2.8mF/cm^2) and cobalt oxide (18mF/cm^2), suggesting the supercapacitive charge injection is intrinsic to the material which in turn could be due to the exposure and availability of more electroactive cations at the interface. This further confirms that the introduction of second transition metal ion to binary metal oxides have a beneficial effect towards supercapacitive charge storage. Galvanostatic charge-discharge cycles at 4mA/cm^2current density using nickel cobaltite nanowires demonstrated extended

cyclability with more than 90% capacity retention at the end of 13000 cycles. Supercapacitive failure mechanism is further investigated by self-discharge and leakage current measurements. Relatively low self-discharge rate (more than 5000s to reach half the initial potential) and leakage current (1.4 $mAF^{-1}V^{-1}cm^{-2}$) in the case of nickel cobaltite nanowires indicate a weaker failure mechanism. A preliminary investigation revealed the dominant failure pathway could be a charge redistribution rather than a diffusion controlled Faradic process. Eventhough the ternary nickel cobaltite nanowires possessed extremely high areal capacitance, its self-discharge rate and leakage currents should be further reduced to improve its supercapacitive characteristics and future investigations in this direction will be beneficial towards making a practical charge storage device.

Future Prospects

Inducing microscopic level off-stoichiometry to the spinel structure may be instrumental in tailoring the electrochemical properties. As off-stoichiometry in general, reflects the preference of the sites, the systematic difference in anti-site occupancies may enhance the charge carriers. It is interesting to understand the effect of site occupancy on supercapacitive properties and the work in this direction is in progress.

Reference

1. Li,D.;Gong,Y.; Zhang,Y.; Luo,C.; Li,W. ; Fu, Q. ; Pan,C.*Sci. Rep.***2015**,*5*, 12903.
2. Shen, L.; Yu,L.; Yu,X.; Zhang,X.;Lou,X.W. *(David) Angew. Chem. Int. Ed.***2015**, *54*, 1868 –1872.
3. Zhang,G. ; Lou and X.W. (David) .*Adv. Mater.***2013***, 25,* 976–979.
4. Yuan,C. ;Li,J. ;Hou,L. ; Zhang,X. ; Shen,L. ;Lou,X.W. (David)*. Adv. Funct. Mater.* **2012** ,*22*, 4592–4597.
5. Yuan,C.; Wu,H.B.; Xie,Y. ;Lou ,X.W. (David).*Angew. Chem. Int. Ed.***2014**,*53,* 1488 – 1504.
6. Wang,R.; Xia,C.;Wei,N.;Alshareef,H.N.*ElectrochimicaActa,***2016**,*196*, 611–621.
7. Zhang,G.Q. ; Wu, H.B.; Hoster,H.E. ; Chan-Park,M.B. ;Lou ,X.W. (David).*Energy Environ. Sci.,***2012***, 5, 9453.*
8. Zhai,Y. ;Mao,H. ; Liu,P.; Ren,X. ; Xu,L. ;Qian,Y. *J. Mater. Chem. A*, **2015**, *3*, 16142
9. Wang,R. ;Yan,X. *Sci. Rep*. **2014**,*4*, 3712
10. Khalid,S. ; Cao,C. ; Wang, L. ; Zhu, Y. *Sci. Rep.***2016**,*6*, 22699
11. Park,M.S. ; Kim,J. ;Kim, J.K. ; Lee,J.W. ; Kim, J.H. ; Yamauchi, Y. *Phys.Chem.Chem.Phys*, **2015** ,*17*, 30963
12. Andreas,H.A.*Journal of The Electrochemical Society*,**2015**,*162* (5) A5047-A5053.
13. Yuan, C. ;Li,J. ; Hou, L. ; Yang, L.; Shen,L. ;Zhang,X. *J. Mater. Chem*., **2012**, *22*, 16084
14. Hung,S.F. ; Tung, C.W. ; Chan, T.S. ; Chen, H.M. *CrystEngComm* , **2016**, *18*,6008

15. Mourad,E.;Coustan,L. ;Lannelongue,P. ;Zigah, D. ; Mehdi,A. ;Vioux,A.Freunberger,S.A. ; Favier,F. ;Fontaine,O. *Nature Materials*. **2016**, 4808

16. Ouyang,A.; Cao,A. ; Hu,S. ; Li,Y. ; Xu,R. ; Wei,J. ; Zhu,H. ;Wu,D. *ACS Appl. Mater. Interfaces,***2016**, *8*, 11179 −11187.

17. Li,X. ; Sun,W. ; Wang,L. ; Qi,Y. ;Guo,T; Zhao,X. ;Yan,X. *RSC Adv*., **2015**, *5*, 7976

18. Voutou,B.; Stefanaki,E.;Giannakopoulos,*K.Physics of Advanced Materials Winter School*,**2008**.

19. Wu,T. ;Li,J. ; Hou ,L. ; Yuan,C. ; Yang,L. ;Zhang,X. *ElectrochimicaActa* ,**2012**, *81*, 172–178.

20. Umeshbabu,E. ;Rajeshkhanna,G. ;Rao,G.R. , *International journal of hydrogen energy*,**2014**,*39* ,15627e15638

21. Wang,Q. ; Liu,B. ; Wang, X. ; Ran,S. ; Wang,L. ;Chen,D. ;Shen.G . *J. Mater. Chem*., **2012**, *22*, 21647.

22. Wang,Q. ;Wang,X.;Liu,B. ; Yu,G. ; Hou,H. ; Chen,D. ;Shen,G. *J.Mater. Chem .A*, **2013**, *1*,2468

23. Zou,R.;Xu,K.;Wang,T.; , He, G. ; Liu, Q.; Liu, X. ;Zhang,Z. ;Ku,J. *J. Mater. Chem***. A**, **2013**, *1* ,8560

24. M.Lukaszewski ; M. Soszko,; A. Czerwinski, *Int. J. Electrochem. Sci.***, 2016 ,***11,*4442 – 4469.

25. Verma,S. ; Kumar,A.; Pravarthana,D.; Deshpande,A.; Ogale,B.S.; Yusuf,M.S.; *J.Phys.Chem. C.***2014**, *118(29),* 16246-16254.

26. Zhu,C, ; Yang,p. ; Chao,D. ; Wang,X. ; Zhang,X. ; Chen,S. ; Tay,B.K. ; Huang,H. ; Zhang,H. ; Mai,W. ;Fan,H.J. *, Adv. Mater.* **2015**, *27*, 4566–4571